vehicles

MDPI

Article

Bending Fatigue Behavior Analysis and Fatigue Life Prediction of Spot-Welded Steel T-Profiles: An XFEM Analysis

Murat Demiral

College of Engineering and Technology, American University of the Middle East, Egaila 54200, Kuwait; murat.demiral@aum.edu.kw

Abstract: Steel T-profiles are extensively used across various sectors due to their versatility and reliability. Spot welding plays a crucial role in their production. These profiles are subjected to cyclic bending loads in numerous engineering applications. Understanding the failure mechanisms is essential for enhancing fatigue resistance and extending the operational lifespan of spot-welded assemblies. Key aspects include accurately predicting where damage initiates, how it propagates under increasing cyclic loads, and the failure point. For this purpose, XFEM analysis was conducted and validated with experimental results from the literature. The study emphasizes the significant impact of bending moment magnitude, load ratio, the diameter of spot welds, and component thickness on the fatigue performance of spot-welded assemblies under bending loads. All these parameters significantly affected the fatigue response. Notably, thinner components showed 8.55 times faster crack propagation, accompanied by more localized and severe cracking.

Keywords: cyclic bending loads; XFEM analysis; spot weld diameter; failure mechanisms; component thickness

Citation: Demiral, M. Bending Fatigue Behavior Analysis and Fatigue Life Prediction of Spot-Welded Steel T-Profiles: An XFEM Analysis. *Vehicles* **2024**, *6*, 2195–2208. https://doi.org/10.3390/vehicles6040107

Academic Editor: Lihui Zhao

Received: 22 October 2024
Revised: 17 December 2024
Accepted: 18 December 2024
Published: 20 December 2024

1. Introduction

Spot-welded steel T-profile assemblies are versatile structural elements widely used across various industries and engineering applications due to their strength, durability, and resistance to different loads. These assemblies are designed to withstand cyclic loading conditions resulting from dynamic forces, vibrations, or repeated mechanical operations. Specifically, the automotive, construction, and industrial machinery sectors rely on these assemblies for their ability to handle fatigue loading scenarios [1].

In automotive applications, spot-welded T-profile assemblies are employed in critical components like the vehicle chassis, body structures, and suspension systems. These components are subject to significant fatigue loads during vehicle operation due to road irregularities, cornering, braking, and accelerating forces. For instance, the repetitive dynamic loads experienced by suspension systems during vehicle motion can lead to fatigue damage in spot-welded joints. The fatigue performance of these assemblies is crucial for ensuring vehicle safety, as the failure of critical components may lead to catastrophic outcomes.

In construction, spot-welded T-profile assemblies are frequently used in structural frameworks that experience cyclic wind or seismic loads. These forces, especially in regions prone to frequent earthquakes or high winds, can induce repetitive loading and unloading cycles on the structural members, which may initiate fatigue cracks in spot-welded joints over time. Buildings, bridges, and other infrastructure projects are increasingly being designed to withstand such cyclic loading, and the fatigue resistance of the connections plays a critical role in ensuring the long-term durability and safety of the structure [2].

In the industrial sector, spot-welded assemblies are used in various pieces of machinery and equipment that are subjected to cyclic mechanical operations. Conveyor systems,

machine frames, and support structures are examples of components exposed to cyclic bending forces, which can induce fatigue cracking over extended periods. As the components undergo repetitive stress during normal operation, fatigue can accumulate, particularly in the welded joints, eventually leading to structural failure if not properly addressed. The performance of these assemblies under cyclic loading, therefore, remains a critical area of study to ensure the reliability and longevity of machinery in industrial applications.

Fatigue failure in spot-welded steel T-profile assemblies occurs as a result of the accumulation of damage from fluctuating stress levels. When exposed to cyclic bending loads, alternating tensile and compressive stresses develop in the flanges of the T-profile. Additionally, shear stresses are concentrated in the spot welds, where the connection between the steel sheets experiences significant strain. The repeated application of cyclic stresses can initiate microstructural defects, such as cracks, at critical points in the assembly, including the weld nugget, heat-affected zone (HAZ), and the surrounding base material. Over time, these defects can propagate under continued loading, ultimately leading to the failure of the entire assembly if not detected and mitigated early [3].

The behavior of spot-welded joints under cyclic loading is significantly influenced by various factors, including the quality of the welds, the material properties of the steel sheets, the geometric configuration of the assembly, and the loading conditions. High-quality welds with sufficient fatigue resistance are essential for ensuring the durability of the assembly. The geometry of the joint, including the spacing of the spot welds and the design of the T-profile, also plays a critical role in the distribution of stresses across the assembly. Proper design considerations, such as optimizing weld spacing and joint geometry, can help reduce stress concentrations and extend the fatigue life of the structure.

While spot-welding is a widely adopted method, it introduces challenges in fatigue performance due to the highly localized nature of the welds. The spot welds act as stress concentrators, and the discontinuities in the welded joints lead to complex stress distributions. This complexity makes predicting fatigue life difficult, as the behavior of the structure is influenced by both the local stress concentrations around the welds and the global stress distribution across the assembly. Moreover, the repeated cyclic loading causes progressive damage to accumulate at the welds, further complicating the prediction of fatigue failure.

Despite the importance of fatigue behavior in spot-welded structures, relatively few studies have specifically examined the performance of spot-welded T-profile assemblies under cyclic bending loads. In the existing literature, several researchers have focused on the fatigue behavior of other types of welded joints or assemblies under different loading conditions. For example, Fan et al. [4] investigated the failure mechanism of a novel composite bolted π-joint under bending load using both experimental and numerical methods. Their study highlighted the delamination failure mode of the fillet region in the L-preform of the joint. Similarly, Kardomateas [5] studied the stresses caused by buckling and the cyclic durability of spot-welded connections in beams subjected to both bending and torsional stresses, providing insights into the fatigue performance of such structures.

A comprehensive method for predicting the fatigue life of complex spot-welded structures was presented by Salvini et al. [6], who used actual equivalent radial stress to develop a predictive model. Their approach was applied to a large dataset of fatigue data, demonstrating the effectiveness of their model in forecasting fatigue life. Bambach et al. [7] analyzed the bending moment-rotation characteristics of thin-walled steel spot-welded hat sections commonly used in the automotive industry. Their findings indicated that perforations in the compression flange significantly affect the performance of compact sections, although the impact decreases with increasing slenderness.

Through mechanical testing, microstructure analysis, and finite element simulations, Xu et al. [8] examined the mechanical characteristics and failure processes of resistance spot welds (RSWs), employing a range of steel kinds and thicknesses. The study discovered that coach-peel loads caused the greatest stress concentration, which may have weakened RSW performance, and that mechanical performance trends like shear strength and bending moment coincide with minimum hardness values. The characteristics of ultrasound-resistant spot-welded joints between DP 800 steel and Litecor metal–plastic composites were examined in [9]. Key findings include a thorough metallographic analysis, proof of polymer core separation without diffusion between the metal layers and polypropylene, and insights into fatigue behavior, which show a fatigue shear strength of 70.576 MPa and a boundary between low-cycle and high-cycle fatigue at about 132 MPa. A fractographic study gave a thorough grasp of joint performance under cyclic shear loads by identifying particular fatigue failure mechanisms at various load levels.

Rahman et al. [10] explored the influence of spot weld and sheet thickness on the fatigue life of spot-welded joints. Their research demonstrated that both factors have a significant impact on the fatigue performance of the joint. Building on this, Ertas and Sonmez [11] presented a design optimization technique to maximize the fatigue life of spot-welded joints subjected to axial and transverse loadings. They found that increasing the number of spot welds not only improved fatigue life but also introduced greater complexity into the design process. In another study, Demiral and Duran [12] employed the extended finite element method (XFEM) to model the fatigue failure of spot-welded structures under cyclic tensile loading. Their study examined various cyclic loads, load ratios, and spot weld sizes to evaluate the fatigue behavior of spot-welded joints. In the following recent works, firstly, Liu et al. [13] examined the fatigue behavior of ST12 lap-shear resistance spot-welded joints under various stress ratios. The findings indicate that stress ratios have a major impact on fatigue life. A novel predictive method that takes this effect into consideration was created and tested against experimental data, with good agreement. This technique improves knowledge of how fatigue behaves in spot-welded joints subjected to cyclic loading, where fatigue life is influenced by stress ratios. Pan et al. [14] investigated the high cycle fatigue crack propagation mechanisms in spot-welded DP980 steel used in automobile bodies, which experienced cyclic loading from vibrations that can lead to fatigue failure. The study identified transitions from eyebrow shape to partial plug failures depending on stress levels using 1.2 mm thick galvanized DP980 steel, adjusted welding conditions, and examined failure processes. Segregated zinc was involved in the initiation of cracks at low loads, whereas at high loads, cracks started at welded pre-notches and spread through different microstructural zones in the heat-affected area.

Kanna and Long [15] concentrated on the fatigue behavior of spot-welded joints in steel sheets, focusing on the fatigue testing, life, and failure causes of modern steels. Lin et al. [16] developed a fatigue crack growth model for spot welds based on local stress intensity factor solutions for kinked cracks. Their model suggested that the fatigue lifetimes of spot welds could be predicted using material constants derived from the Paris law for fatigue crack growth. These studies collectively highlight the challenges associated with predicting the fatigue performance of spot-welded structures, particularly when subjected to cyclic bending loads.

The literature review indicates that the performance of spot-welded T-profile assemblies under cyclic bending load has not been studied in depth. Predicting the fatigue performance of spot-welded structures presents a formidable challenge due to the continual redistribution of loads across each spot weld and the subsequent evolution of damage. Additionally, achieving a precise assessment of local stress is intricate given the significant discontinuity experienced by the sheet connections.

To address this, this study presents an XFEM model for the spot-welded assembly under cyclic bending loading, validated using experimental data from two distinct scenarios. Fatigue performance in spot-welded T-profile assemblies depends on multiple factors, including weld quality, material properties, geometric design, and loading conditions. High-quality spot welds with adequate strength and fatigue resistance are essential for enduring cyclic loading without premature failure. Strategic design considerations, like weld spacing and joint geometry, facilitate even distribution of cyclic stresses across the assembly, minimizing stress concentrations and extending fatigue life. An assessment was carried out to ascertain the influence of numerous model parameters, including the diameter of spot welds (D), the applied bending load (F), the thickness of assembly components (t), the load ratio (R), and the presence of a base part on its fatigue behavior.

2. XFEM Modeling

A three-dimensional XFEM model is created in this study to analyze how the spot-welded assembly responds to cyclic bending loads. The Abaqus 2021 FE software [17] was employed for constructing the model. The geometric characteristics of the assembly's constituent parts are illustrated in Figure 1, comprising four primary sections. Throughout the fatigue loading process, Parts A and B, serving as the primary components, receive support from Parts C and D, respectively.

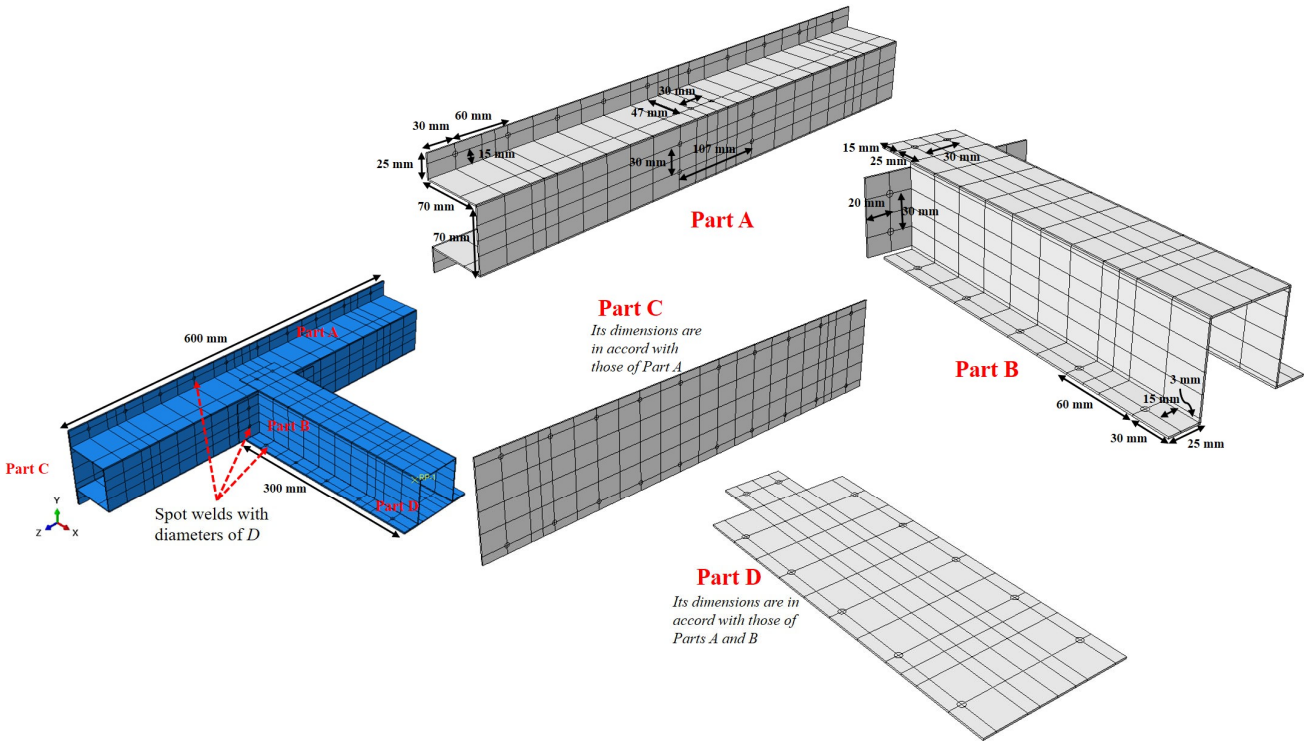

Figure 1. Geometric information on the T-profile assembly's component parts.

Figure 2 displays the specifics of the developed XFEM model. The assembly was exposed to bending moment M applied from the free ends of Parts B and D, each with a length of 40 mm. Meanwhile, Parts A and C were fixed in all directions in regions with lengths of 70 mm close their respective free ends. M was applied to the reference point (RP-1) depicted in Figure 2, positioned at the geometric center in the y- and z- directions and 60 mm in the x-direction from the loaded portion of the structure. RP-1 controlled the relevant region using a coupling constraint defined in the model. XFEM was primarily applied to the areas of the parts connected via spot welds, aligning with findings in the existing literature indicating that cracks primarily originate and propagate around spot welds in the structure. Utilizing Abaqus' tie constraint module, the part interfaces on the

welding side were labeled as master and slave surfaces to mimic spot welding. A total of 38 spot welds were utilized to combine the various parts to make the assembly: 20 welds joined Parts A and C, 10 welds joined Parts B and D, 6 spot welds united Parts A and B, and 2 spot welds fused Parts A and D together.

Employing 25 Fourier terms, a direct cycle analysis was conducted to replicate the fatigue loading with a load ratio of −1. To initiate crack formation in stress concentration areas, M was applied to the structure in a separate static step preceding the loading cycle.

The mesh details used in the model are depicted in Figure 2. To ensure the model's accuracy, a mesh convergence analysis was undertaken. Three simulations were executed when the assembly underwent the bending moment, utilizing three distinct mesh sizes ranging from 0.3125 mm to 1.25 mm. The highest von Mises stress value observed in the element adjacent to the welding zones was compared across each model. When transitioning from a mesh size of 0.625 mm to 0.3125 mm, the discrepancy observed was less than 3.46%, while the transition from the coarsest to the medium mesh resulted in a difference of over 8.95%. Consequently, the model was discretized using element sizes of 0.625 mm. It is important to note that since XFEM results are unaffected by the mesh size used, the mesh study was specifically conducted for the static analysis simulating crack formation. For discretization, eight-noded linear brick elements with reduced integration (C3D8R) were employed.

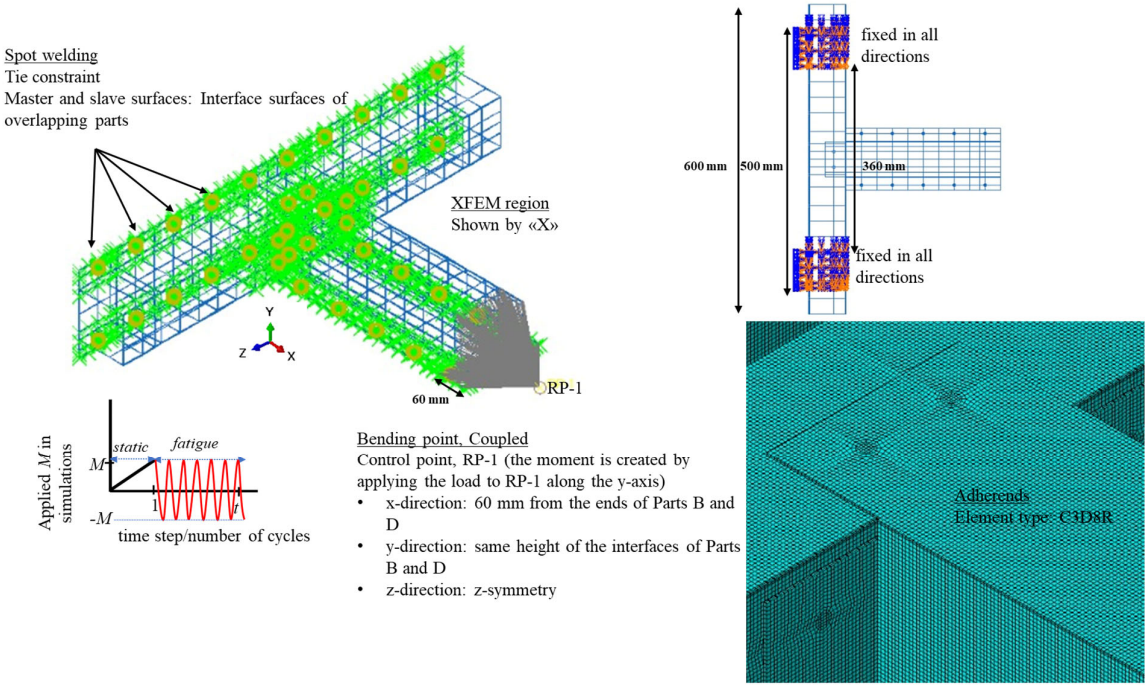

Figure 2. Information regarding the T-profile assembly's XFEM modeling under cyclic bending stress.

XFEM is a computational technique developed to address crack propagation challenges within the framework of the traditional finite element method (FEM). Its flowchart is shown in Figure 3. It expands upon classical FEM by incorporating the concept of partition of unity, allowing for the seamless integration of localized enrichment functions into the finite element approximation. This integration is facilitated by specialized enriched functions along with additional degrees of freedom, ensuring the presence of discontinuities within the model. Unlike conventional methods, XFEM simulations of crack propagation do not necessitate predefined crack paths or initial crack definitions that conform to the structural mesh. Instead, the crack path emerges as part of the solution process. When it comes to fracture analysis, the enrichment functions usually comprise a discontinuous function that represents the displacement leap over the crack surfaces and near-tip asymptotic functions that capture the singularity close to the crack tip (Equation (1)).

In XFEM, the representation of a displacement vector function with partition of unity enrichment is as follows:

$$u(x) = \sum_{I \epsilon N} N_I(x) \left[u_I + H(x)\alpha_I + \sum_{\alpha=1}^{4} F_\alpha(x) b_I^\alpha \right] \quad (1)$$

In this expression, $N_I(x)$ represents the standard nodal shape functions; u_I denotes the usual nodal displacement vector corresponding to the continuous component of the finite element solution. The second component entails the multiplication of the nodal-enriched degree of freedom vector, a_I, with the corresponding discontinuous jump function $H(x)$ across the crack surfaces. The third component involves the multiplication of the nodal-enriched degree of freedom vector, b_I^α, with the associated elastic asymptotic crack-tip functions, $F_\alpha(x)$. In this study, the necessity for near-tip asymptotic singularities is circumvented, focusing solely on the displacement jump across a cracked element [17].

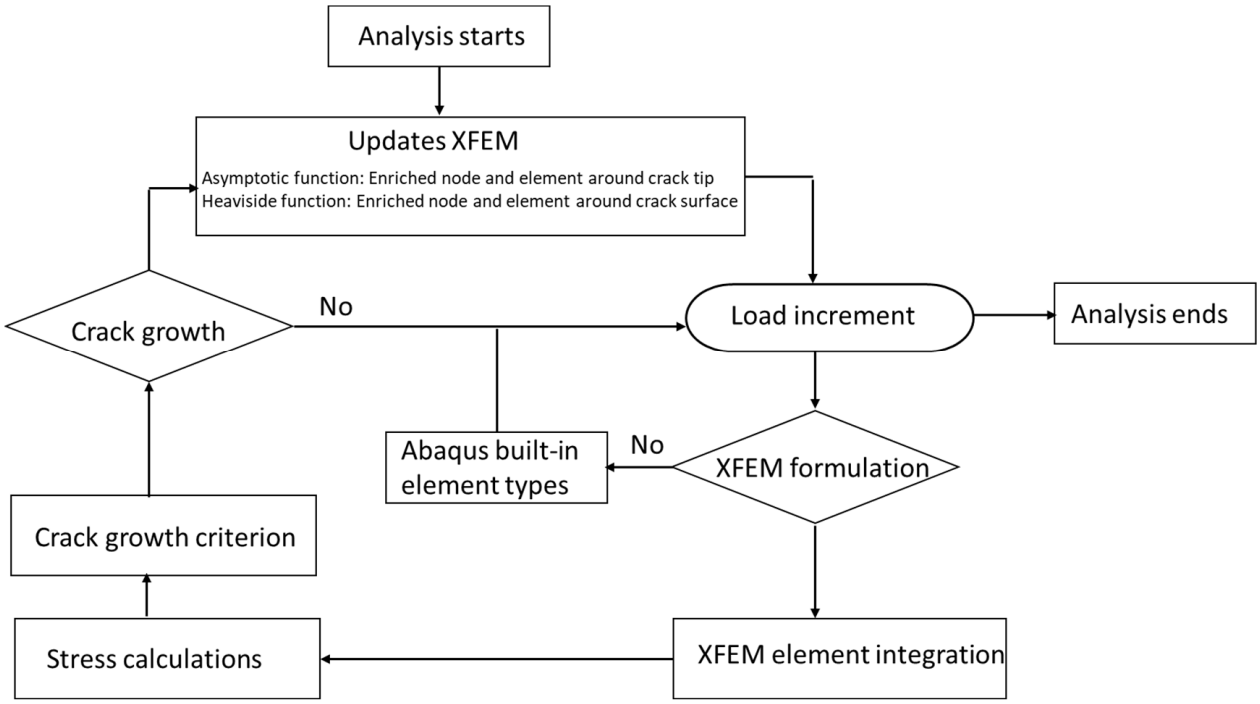

Figure 3. The flowchart of XFEM [17].

The simulations utilized the direct cyclic method within Abaqus/Standard, integrating both XFEM and linear elastic fracture mechanics (LEFMs). The initiation and progression of the crack were simulated using the Paris law, which correlates the rate of crack growth with the fracture energy release rate. Definitions were set for the maximum energy release rate (G_{pl} = 0.85 $G_{eq,\,c}$) and the lower threshold (G_{thresh} = 0.01 $G_{eq,\,c}$). $G_{eq,\,c}$ denotes the critical equivalent strain energy release rate, determined using the mode-mix criterion and calculated employing the linear power law model.

$$\frac{G_{eq}}{G_{eq,\,c}} = \left(\frac{G_1}{G_{1c}}\right)^{\alpha_1} + \left(\frac{G_2}{G_{2c}}\right)^{\alpha_2} + \left(\frac{G_3}{G_{3c}}\right)^{\alpha_3} \quad (2)$$

The opening (Mode I), first shear (Mode II), and second shear (Mode III) critical energy release rates in this model are indicated as G_{1c}, G_{2c}, and G_{3c}, respectively. For analysis, the coefficients α_1, α_2 and α_3 are taken to have a value of 1.0. The low-cycle fatigue research uses ΔG, which represents the difference in energy release rates between minimum and maximum loads, to quantify fatigue fracture in the structure. The crack growth rate per cycle is calculated using the Paris law, expressed as $da/dN = c_3\Delta G^{c_4}$, where a represents crack length, N is the cycle number, and c_3 and c_4 are material constants. To accurately depict crack initiation and progression, the condition $G_{pl} > G_{max} > G_{thresh}$ must be satisfied in computations.

Upon crack initiation, the following steps are taken: one element is released at the interface at the end of each cycle N, progressively advancing the crack length (a_N) from the current cycle to $a_{N+\Delta N}$. ΔN_j, where j corresponds to the node at the crack tip, represents the cycles required for failure in each interface element. Node spacing at interface elements near crack tips ($\Delta a_{Nj} = a_{N+\Delta N} - a_N$) and material constants c_3 and c_4 are utilized in this calculation. The objective is to release one or more interface elements at the end of each stable loading cycle. Hence, $\Delta N_{min} = \min(\Delta N_j)$ is determined as the number of cycles necessary for crack propagation across its element length, with $\Delta a_{Nmin} = \min(\Delta a_{Nj})$ identifying the element requiring the fewest cycles for propagation. Upon finding the element necessitating the fewest cycles, zero stiffness and constraint are achieved, and the next cycle releases the interface element, computing a new relative fracture energy release rate for interface elements at the crack tip according to [17,18].

The material constants used in simulations are listed in Table 1, encompassing elastic modulus, Poisson's ratio, tensile strength, critical energy release rates in various modes (G_{1c}, G_{2c} and G_{3c}), and material constants utilized in the Paris law (c_3 and c_4).

Table 1. The EN 10,130 low-carbon steel material parameters utilized in the simulations.

[19]			[12]		
E (MPa)	v	TS (MPa)	G_{1c}, G_{2c}, G_{3c} (N/m)	c_3	c_4
210,000	0.3	326	6500	7.5×10^{-8}	1.75

3. Results and Discussion

This section presents first the numerical model's validation utilizing the assembly's failure cycles (N_f) that were obtained experimentally. The impact of many parameters, including the nugget diameter, the thickness of the parts in the assembly, the amount of torque, the presence of the base in terms of N_f, the site of the crack initiation, and its spread in a row, are further examined. Discussions that are pertinent are also included.

3.1. Validation of the Numerical Model

For validating the developed XFEM model, the experimental data from [20] were utilized. The spot-welded assembly was examined in two different configurations. In the first configuration, the nugget diameter and the part thickness were 5.5 mm and 1.5 mm, respectively; in the second one, these measurements were 6.5 mm and 2.0 mm. The assembly was subjected to a bending moment with loads of 700 N and 850 N, respectively. Table 2 presents the number of failure cycles (N_f) obtained from both numerical analysis and experimental observations. Experimentally, increasing the thickness from 1.5 mm to 2.0 mm raised the failure cycles from 225,000 to 440,000. Numerically, the corresponding values were 270,210 and 444,940 cycles. The results were in good agreement. The outcomes of the FE simulations using the stiff spot weld model were also provided in [20]. In this model, bar elements with a rigid formulation were employed at the nugget area to connect the sheets, while quad elements were used to mimic the spot-welded regions on the sheet metals [19]. The corresponding FE simulations predicted the N_f of the cases poorly, at 24,300 and 48,500 cycles, respectively. The XFEM simulations provided a more accurate prediction of the experimental results compared to FEM. The ability of crack growth observation

in XFEM was another advantage against the FE predictions [18]. During the resistance spot-welding process, the heat-affected zone and base material are separate areas that develop as a result of localized heating. The region next to the weld nugget that experiences heat cycles but does not melt is known as the HAZ. High temperatures are applied to it, changing its mechanical characteristics and microstructure, resulting in variations in strength and hardness. The variations in the mechanical characteristics of the base material, HAZ, and weld nugget were not considered in the XFEM simulations in accordance with the research in the literature [12,18,19]. Additionally, the impact of fatigue loading-induced energy dissipation was not taken into account by the model. These points may contribute to the discrepancy between the experimental and numerical values of N_f obtained here.

Figure 4 presents the formed cracks leading to the assembly's failure for two configurations. In the first one, the cracks emerged and grew in Part A around the spot welds connecting Parts A and D on both sides and also in Part B connecting Parts A and B on the right side only. In the latter, different crack patterns were noted, where the cracks formed in both Parts A and B around the spot welds connecting these two parts and also in Part D connecting Parts A and D on both sides. The experimentally observed crack propagation is shown in Figure 5. In Ref. [20], only the crack formed around the spot weld connecting Parts A and B was presented; no information about the other cracks was given.

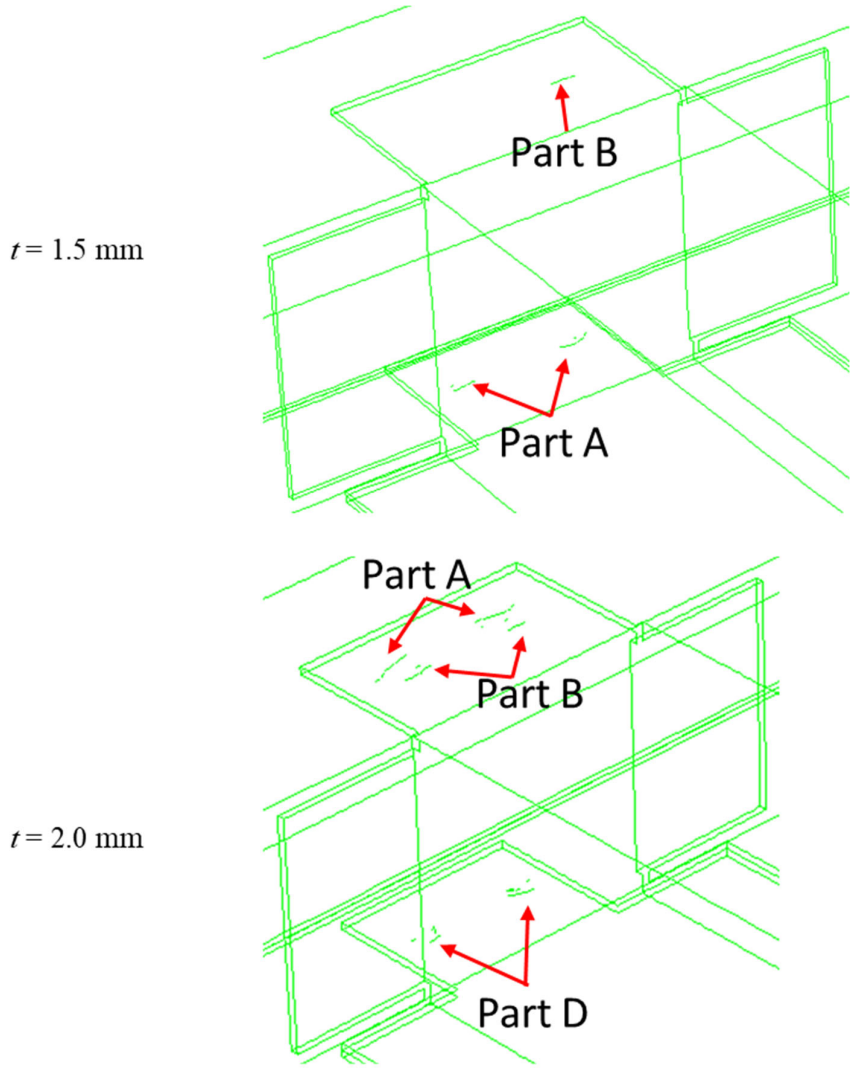

Figure 4. The formed cracks in the assembly for t = 1.5 and 2.0 mm when N_f is reached.

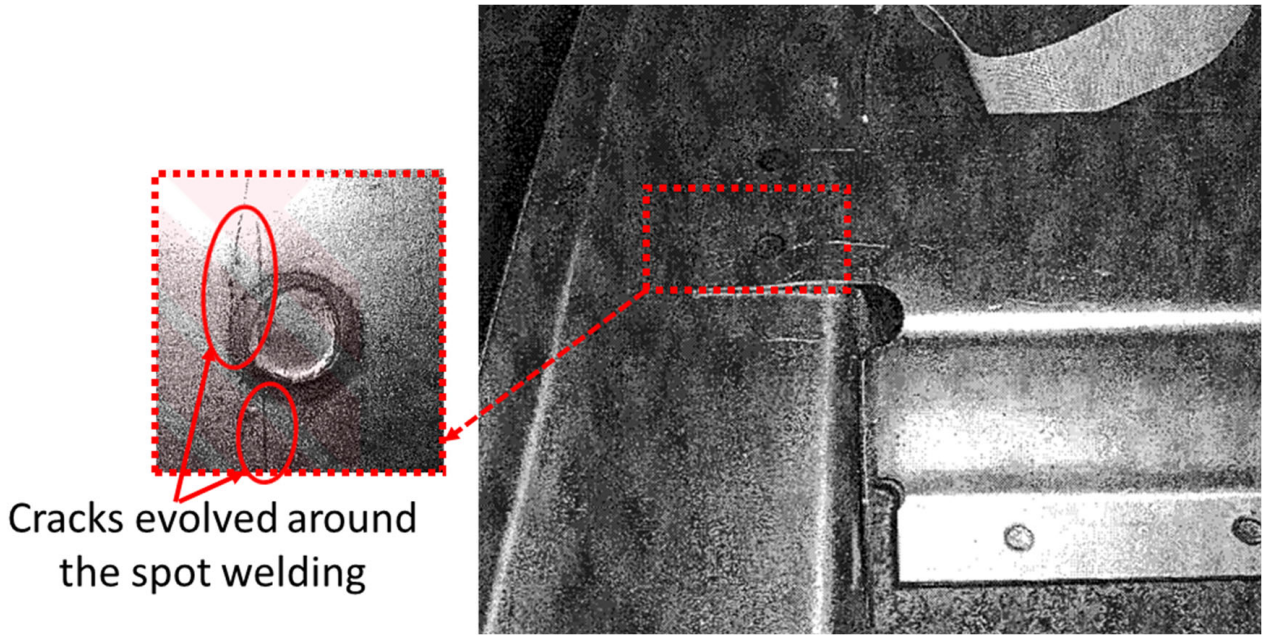

Figure 5. The crack pattern around the spot weld observed experimentally [20].

Table 2. Failure cycles obtained both numerically and experimentally for two distinct scenarios.

			Experiments [20]	**FEM–Rigid Spot Weld Model [20]**	**XFEM**
t (mm)	D	F		N_f	
1.5	5.5	±700 N	225,000	24,300	270,210
2.0	6.5	±850 N	440,000	48,500	444,940

3.2. Influence of the Diameter of Spot Welds

One variable that could influence the bending performance of the assembly is the diameter of the spot weld. This study examined three scenarios, adjusting the diameter from 4.5 mm to 6.5 mm in 1.0 mm increments, while keeping the thickness constant at 1.5 mm. The corresponding N_f and the average crack propagation rate (da/dN) are presented in Table 3. As the diameter enlarged from 4.5 mm to 6.5 mm, N_f rose to 48,914, 270,210, and 442,380, respectively, with N_f increasing by 5.52 and 1.63 times as the diameter increased by 1.22 and 1.18 times. The average crack propagation rate was calculated for each configuration using $(a_f - a_0)/N_f$, where a_0 and a_f represent the crack lengths at the end of the static cycle and at $N = N_f$, respectively. This rate decreased from 1.53×10^{-4} mm/cycle to 2.16×10^{-5} mm/cycle, a reduction of about 7.1 times, as the diameter increased from 4.5 mm to 6.5 mm. It was determined that when the nugget's diameter shrank, the crack propagated more quickly because the smaller spot-welding size could not assemble the parts adequately. In this case, it was found that the spot weld's size had a major impact on the structure's fatigue performance. This is in line with what was shown in [21], where longer fatigue lives were achieved by larger nugget diameters because of the notch effect. This resulted in lower strains and stresses developing close to the spot-welding site, which decreased the likelihood that fractures would emerge.

Table 3. N_f and *da/dN* for varying spot weld diameters obtained from XFEM.

T (mm)	*D* (mm)	N_f (cycles)	*da/dN* (mm/Cycle)
1.5	4.5	48,914	1.53×10^{-4}
	5.5	270,210	3.41×10^{-5}
	6.5	442,380	2.16×10^{-5}

Figure 6 shows the resulting crack patterns for each configuration when N reaches N_f cycles. It was observed that when D was equal to 4.5 mm, the cracks were observed only in Parts A and B around the spot welds connecting these two parts. A similar pattern was noticed for when D was equal to 6.5 mm, where additional cracks were observed in Part D around the spot welds connecting Parts A and D. However, a different crack distribution was noticed when D became 5.5 mm. Only on the right-side spot weld in Part B connecting Parts A and B as well as around two spot-welds in Part A connecting Parts A and D were the cracks formed.

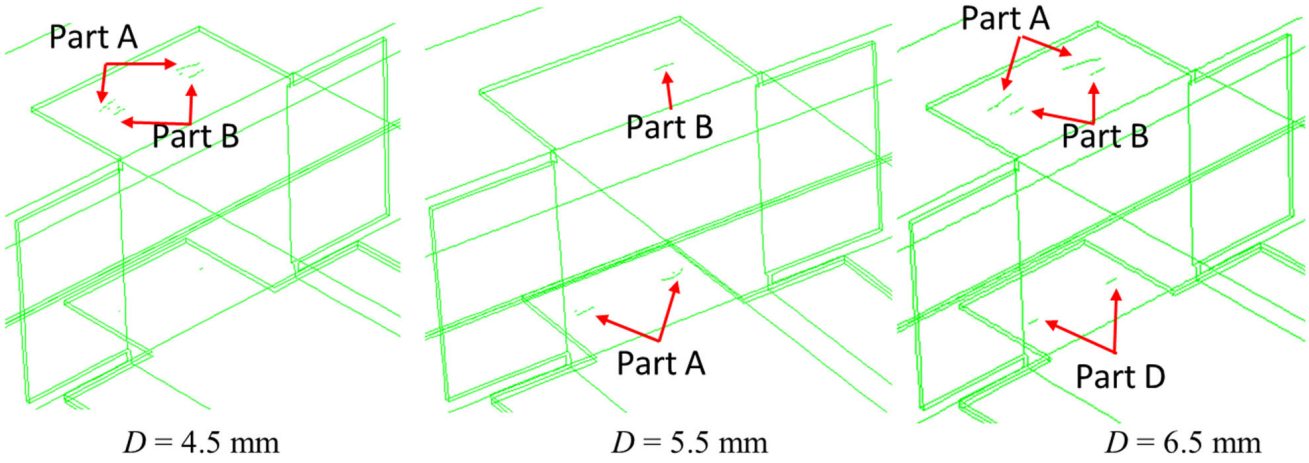

Figure 6. A depiction of the cracks within the assembly upon reaching N_f for various spot weld diameters.

3.3. Influence of Thickness

Second, a study was conducted to determine how a spot-welded box's torsional fatigue life is impacted by the thickness of its assembly components. The thickness was changed from 1.0 mm to 2.0 mm in increments of 0.5 mm. Figure 7 displays the N_f values obtained: 54,929, 270,210 and 440,310 cycles, respectively. With a thickness of 1.0 mm, the N_f was over eight times lower compared to that with a thickness of 2.0 mm, indicating a weaker structure where cracks propagated more rapidly under bending stress (the average *da/dN* increased more than 8.55 times from 2.01×10^{-5} to 1.72×10^{-4} mm/cycle), resulting in shorter fatigue life. Figure 8 shows the crack patterns after reaching N_f for each thickness. At 1.0 mm, cracks appeared only in Parts A and B around the spot welds connecting them. When increased to 2.0 mm, cracks also formed around the spot welds in Part D connecting Parts A and D and on the right-side spot welds in Parts A and B. Thus, component thickness significantly influences the failure pattern of the assembly under bending load.

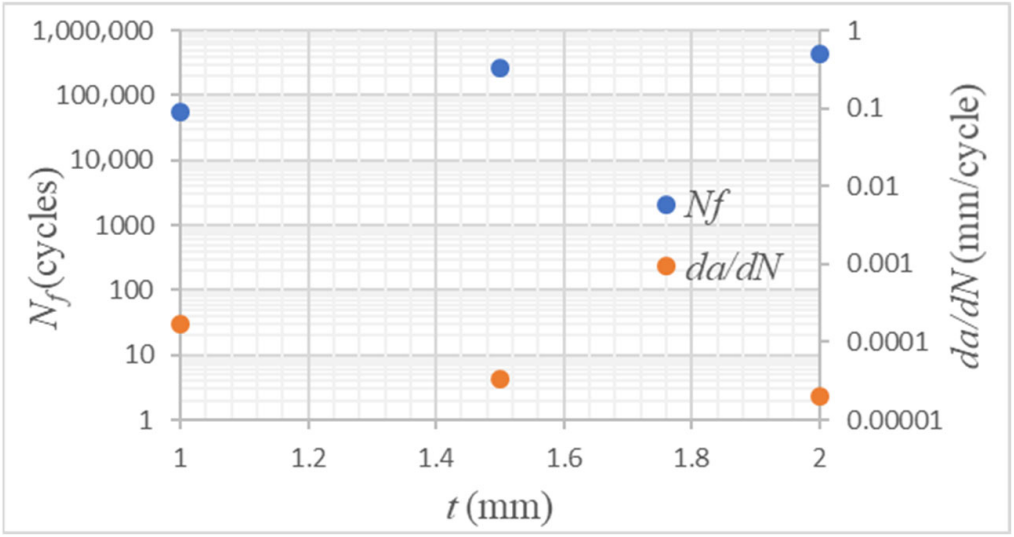

Figure 7. N_f and *da/dN* versus the thickness of the parts.

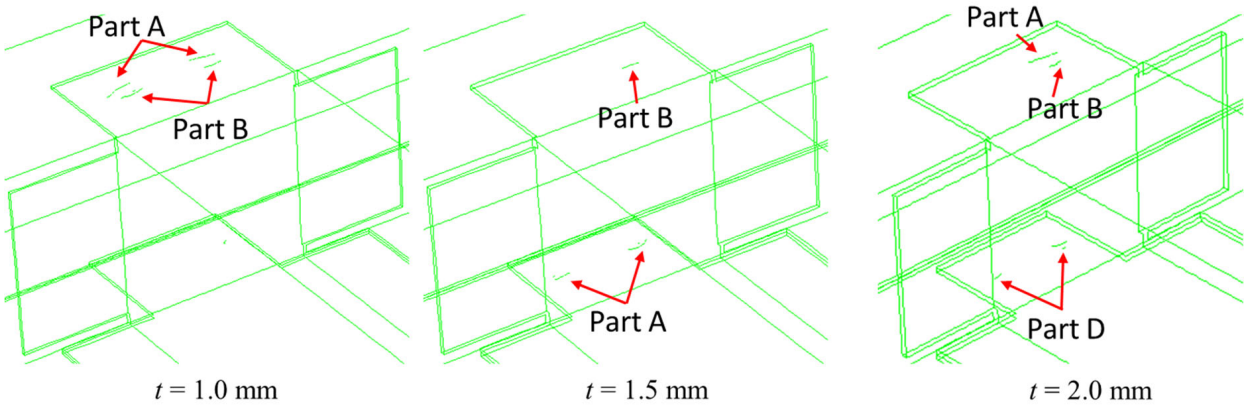

Figure 8. The cracks formed within the assembly for various *t* values at $N = N_f$.

3.4. Effects of the Bending Moment Amount and the R

Lastly, this study examined the effects of bending moment magnitude and the load ratio *R*. The bending moment was altered by adjusting *F* to ±500 N and ±900 N from the reference value of ±700 N. Table 4 displays the resulting N_f and *da/dN* values. It was found that N_f almost halved from 270,210 to 138,220 cycles when *F* was increased to ±900 N compared to the reference, while an infinite fatigue life was observed for *F* at ±500 N. In this context, a fatigue life exceeding 10^6 cycles was considered to reach the run-out threshold. The average *da/dN* rose from 3.41×10^{-5} to 6.91×10^{-5} mm/cycle when *F* was increased from ±700 N to ±900 N. Figure 9 illustrates the resulting crack patterns for the examined cases, revealing similar crack patterns regardless of the applied *F* magnitude. The crack lengths for *F* = ±500 did not reach the required size for 10^6 cycles, thus marking an infinite fatigue life.

The load ratio *R* was another critical parameter affecting fatigue performance. When *R* was adjusted from −1.0 to −0.75, an infinite fatigue life was observed for the latter, as shown in Table 4, with a similar crack pattern evident in Figure 9.

Table 4. Numerically obtained N_f and *da/dN* for different *F* and *R* values.

F (N)	*R*	N_f	*da/dN* (mm/Cycle)
±500 N	−1.0	10^6	-
±700 N	−1.0	270,210	3.41×10^{-5}
±900 N	−1.0	138,220	6.91×10^{-5}
−525 N, 700 N	−0.75	10^6	-

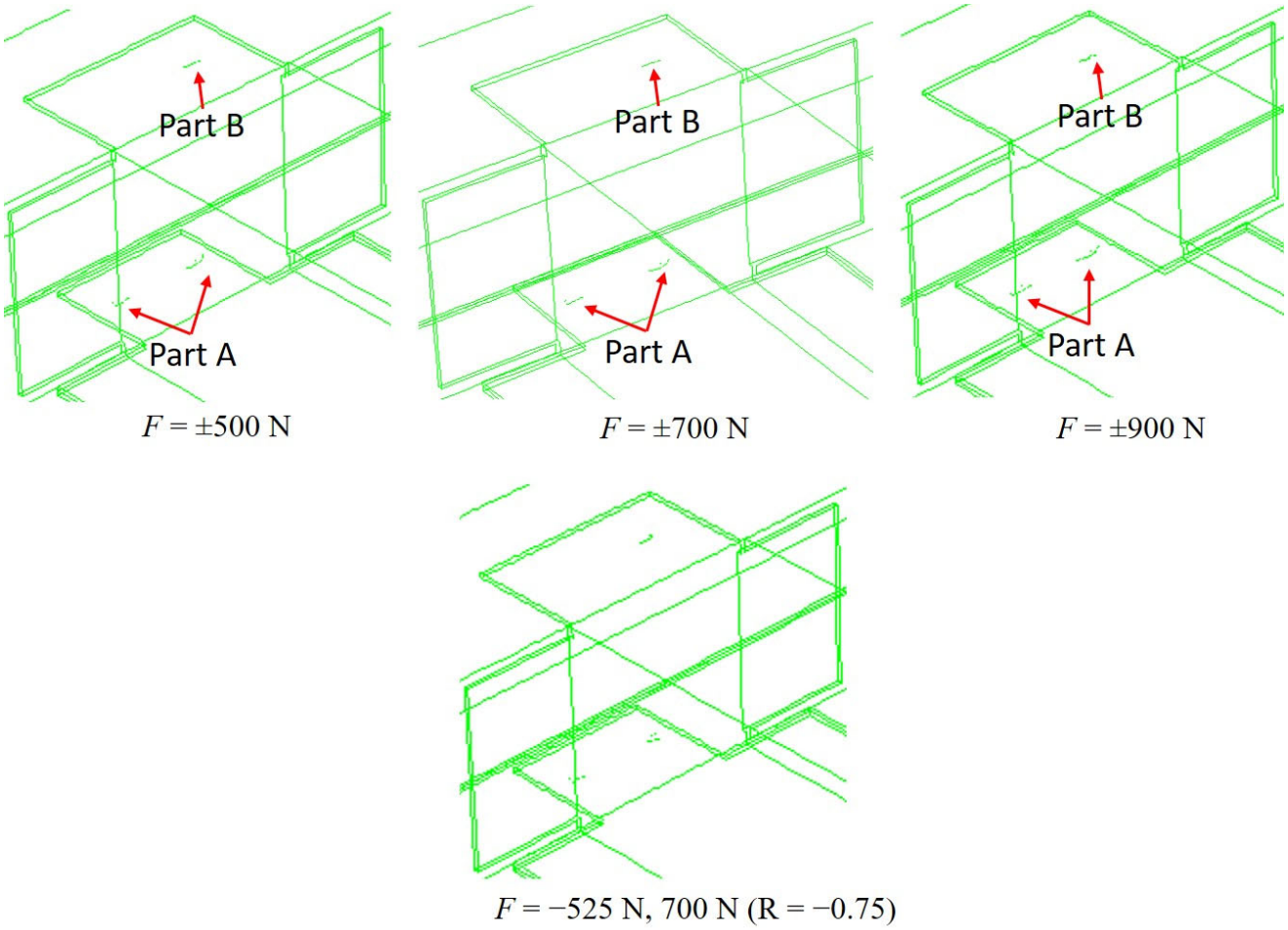

Figure 9. The formed cracks within the assembly for different *F* and *R* values at $N = N_f$.

4. Conclusions

This numerical research looked at a number of important parameters related to the assembly's fatigue failure under bending stresses. XFEM was used to model the propagation of cracks, and the model's validity was confirmed by published experimental data. The following deductions were made:

- Increasing the spot weld diameter from 4.5 mm to 6.5 mm significantly improved fatigue performance, raising N_f by up to 5.52 times and reducing the average *da/dN* by 7.1 times. Larger diameters reduced the notch effect, lowering strains and stresses near the weld, thus decreasing fracture initiation. Crack patterns confirmed more severe cracking with smaller diameters.

- Improved torsional fatigue life was observed with a considerable increase in component thickness from 1.0 mm to 2.0 mm, with N_f for 1.0 mm being over eight times lower. Thinner components had faster average crack propagation (*da/dN* increased 8.55 times) and more localized, severe cracking, while thicker components showed distributed crack formation.
- Both bending moment magnitude and load ratio R significantly affect fatigue performance. Increasing F from $\pm$700 N to $\pm$900 N halved N_f and doubled the average *da/dN*. Reducing F to $\pm$500 N led to infinite fatigue life. Changing R from -1.0 to -0.75 also resulted in infinite fatigue life. Crack patterns were similar regardless of F or R values.

Funding: The APC was funded by the American University of the Middle East, Kuwait.

Data Availability Statement: Data sets generated during the current study are available from the corresponding author on reasonable request.

Conflicts of Interest: The authors declare no conflict of interest.

References

1. Yokoyama, Y.; Nagasaka, K.; Masuda, I.; Sugiyama, H.; Okazawa, S. Simulation of Automobile Structural Member Deformation and Crash via Isogeometric Analysis. *Vehicles* **2024**, *6*, 967–983. [CrossRef]
2. Maquin, F.; Pierron, F. Heat dissipation measurements in low stress cyclic loading of metallic materials: From internal friction to micro-plasticity. *Mech. Mater.* **2009**, *41*, 928–942. [CrossRef]
3. Narimani, M.; Hajjari, E.; Eskandari, M.; Szpunar, J.A. Elevated temperature tensile behavior of S900 HSLA steel and its welded joints. *J. Constr. Steel Res.* **2023**, *203*, 107782. [CrossRef]
4. Fan, J.; Cheng, X.; Wang, S.; Guo, X.; Zhang, T. Experimental and numerical investigation of composite bolted π-joint subjected to bending load. *Compos. Part B Eng.* **2015**, *78*, 324–330. [CrossRef]
5. Kardomateas, G.A. Spot weld failure from buckling-induced stressing of beams under cyclic bending and torsion. *Eng. Fract. Mech.* **1992**, *42*, 519–530. [CrossRef]
6. Salvini, P.; Vivio, F.; Vullo, V. Fatigue life evaluation for multi-spot welded structures. *Int. J. Fatigue* **2009**, *31*, 122–129. [CrossRef]
7. Bambach, M.R.; Tan, G.; Grzebieta, R.H. Steel spot-welded hat sections with perforations subjected to large deformation pure bending. *Thin-Walled Struct.* **2009**, *47*, 1305–1315. [CrossRef]
8. Xu, Z.; Tian, C.; Mao, L.; Tian, H.; Yi, B.; Ling, H. A mechanical properties and failure mechanism study for resistance spot welded AHSSs under coach-peel and lap-shear loads. *Eng. Fract. Mech.* **2023**, *290*, 109474. [CrossRef]
9. Kubit, A.; Derazkola, H.A.; Faes, K.; Korzeniowski, M. Fatigue properties of spot joints of metal-plastic composites with DP 800 steel prepared by ultrasound resistance spot welding. *Thin-Walled Struct.* **2024**, *201*, 111992.
10. Rahman, M.M.; Rosli, A.B.; Noor, M.M.; Sani, M.S.; Julie, J.M. Effects of spot diameter and sheets thickness on fatigue life of spot welded structure based on fea approach. *Am. J. Appl. Sci.* **2009**, *6*, 137. [CrossRef]
11. Ertas, A.H.; Sonmez, F.O. Design optimization of spot-welded plates for maximum fatigue life. *Finite Elem. Anal. Des.* **2011**, *47*, 413–423. [CrossRef]
12. Demiral, M.; Duran, E.T. Failure Analysis of Resistance Spot-Welded Structure Using XFEM: Lifetime Assessment. *Appl. Sci.* **2023**, *13*, 10923. [CrossRef]
13. Liu, H.; Huo, X.H.; Zhang, Z.H.; Yan, W.K.; Zhang, D.D. A Fatigue Life Prediction Approach for Resistance Spot Welded Joints with Consideration of the Stress Ratio Effect. *J. Mater. Eng. Perform.* **2024**, 1–8. [CrossRef]
14. Pal, B.; Amirthalingam, M.; Raman, S.G. An Experimental Investigation on the High Cycle Fatigue Behavior of Resistance Spot Welded Ultrahigh Strength Steel. *J. Mater. Eng. Perform.* **2023**, *33*, 12906–12916. [CrossRef]
15. Khanna, S.K.; Long, X. Fatigue behavior of spot welded joints in steel sheets. In *Failure Mechanisms of Advanced Welding Processes*; Woodhead Publishing: Sawston, UK, 2010; pp. 65–100.
16. Lin, S.H.; Pan, J.; Wung, P.; Chiang, J. A fatigue crack growth model for spot welds under cyclic loading conditions. *Int. J. Fatigue* **2006**, *28*, 792–803. [CrossRef]
17. Systèmes, D. *Abaqus Documentation*; Dassault Systèmes: Providence, RI, USA, 2021.
18. Duran, E.T.; Demiral, M. Comparing and validating the numerical modeling of spot-welded fatigue failure using FEM and XFEM methods for HCF. *Eng. Fail. Anal.* **2024**, *158*, 108049. [CrossRef]
19. Duran, E.T. Finite element based Multi-Axial low cycle fatigue analyses of Spot-Welded components and correlation with tests. *Eng. Fail. Anal.* **2022**, *132*, 105899. [CrossRef]

20. Dincer, S. A Comparative Study on the Finite Element Models for Spot Welds and Their Verification. Master's Thesis, Istanbul Technical University, Istanbul, Turkey, 2005.
21. Ertas, A.H.; Sonmez, F.O. A parametric study on fatigue strength of spot-weld joints. *Fatigue Fract. Eng. Mater. Struct.* **2008**, *31*, 766–776. [CrossRef]